International Journal of Nanomedicine

Dovepress

open access to scientific and medical research

Open Access Full Text Article

ORIGINAL RESEARCH

Combined Ferromagnetic Nanoparticles for Effective Periodontal Biofilm Eradication in Rat Model

Fei Tong[1–4], Pei Wang[1,3,4], Ziqiang Chen[1,3,4], Yifan Liu[1,3,4], Lianguo Wang[1,3,4], Jun Guo[1,3,4], Zhihua Li[1,3,4], Hu Cai[2,4], Junchao Wei[1–4]

[1]School of Stomatology, Nanchang University, Nanchang, 330006, People's Republic of China; [2]School of Chemistry and Chemical Engineering, Nanchang University, Nanchang, Jiangxi Province, 330031, People's Republic of China; [3]The Key Laboratory of Oral Biomedicine, Nanchang, Jiangxi Province, 330006, People's Republic of China; [4]Jiangxi Province Clinical Research Center for Oral Diseases, Nanchang, 330006, People's Republic of China

Correspondence: Hu Cai, School of Chemistry and Chemical Engineering, Nanchang University, 999# Xuefu Road, Honggutan District, Nanchang, Jiangxi, 330031, People's Republic of China, Tel +86 791 83969514, Email caihu@ncu.edu.cn; Junchao Wei, School of Stomatology, Nanchang University, 49# Fuzhou Road, Donghu District, Nanchang, Jiangxi, 330006, People's Republic of China, Tel +86 791 86236950, +86 791 6361141, Email weijunchao@ncu.edu.cn

Introduction: The critical challenge for periodontitis therapy is thoroughly eliminating the dental plaque biofilm, particularly penetrating the deep periodontal tissue. Regular therapeutic strategies are insufficient to penetrate the plaque without disturbing the commensal microflora of the oral cavity. Here, we constructed a Fe_3O_4 magnetic nanoparticle loading minocycline (FPM NPs) to penetrate the biofilm physically and effectively eliminate periodontal biofilm.

Methods: In order to penetrate and remove the biofilm effectively, Fe_3O_4 magnetic nanoparticles were modified with minocycline using a co-precipitation method. The particle size and dispersion of the nanoparticles were characterized by transmission electron microscopy, scanning electron microscopy, and dynamic light scattering. The antibacterial effects were examined to verify the magnetic targeting of FPM NPs. Confocal laser scanning microscopy was employed to check the effect of FPM + MF and develop the best FPM NPs treatment strategy. Additionally, the therapeutic effect of FPM NPs was investigated in periodontitis rat models. The expression of IL-1β, IL-6, and TNF-α in periodontal tissues was measured by qRT-PCR and Western blot.

Results: The multifunctional nanoparticles exhibited intense anti-biofilm activity and good biocompatibility. The magnetic forces could pull FMP NPs against the biofilm mass and kill bacteria deep in the biofilms both in vivo and in vitro. The integrity of the bacterial biofilm is disrupted under the motivation of the magnetic field, allowing for improved drug penetration and antibacterial performance. The periodontal inflammation recovered well after FPM NPs treatment in rat models. Furthermore, FPM NPs could be monitored in real-time and have magnetic targeting potentials.

Conclusion: FPM NPs exhibit good chemical stability and biocompatibility. The novel nanoparticle presents a new approach for treating periodontitis and provides experimental support for using magnetic-targeted nanoparticles in clinic applications.

Keywords: ferromagnetic nanoparticle, periodontitis, biofilm, magnetic targeting

Introduction

Periodontal diseases are chronic oral inflammatory conditions triggered by the imbalance between resident subgingival microbiota and the host's immune response. The progression of the disease can lead to improper positioning of the jaws and supporting tissues, even leading to the loss of teeth.[1–3] A couple of associated conditions were reported to be accompanied by periodontitis, such as stroke,[4,5] myocardial infarction,[6,7] atherosclerosis, hypertension,[8,9] and cancer.[10,11] Generally, the colonization of certain anaerobic subgingival bacteria, including *P. gingivalis, Treponema denticola*, and *Tannerella forsythia*, is widely accepted as the primary cause of periodontal diseases.[12] As a coating, plaque can be constantly generated by these bacteria using the sugars in the foods and drinks consumed. Most biofilms are difficult to remove, and drug permeability can be poor due to the barrier, which also increases the production of antimicrobial resistance. The sticky film of bacteria will result in sore, bleeding gums and painful chewing problems, eventually leading to tooth loss.[3] The

Received: 9 January 2023
Accepted: 26 April 2023
Published: 9 May 2023

elimination of the dental plaque biofilm is difficult due to the polysaccharide matrix. Indeed, inhibition of bacterial biofilms often requires antibiotics doses up to 1000 times higher than those of suspended bacteria.[13,14]

Bacterial biofilms have been shown to affect drug delivery directly. The association of bacterial biofilms with periodontitis makes clarifying and understanding their underlying formation mechanisms important.[1,15] Several studies have been conducted to evaluate robust anti-biofilm activity tools, including nanoparticles.[16–20] However, one critically important, yet often overlooked, obstacle of these treatments is the bacterial biofilms, primarily composed of attached microbial cells encased within a matrix of extracellular polymeric secretions (EPS). The complex biochemical components of biofilms have made them difficult to break down. Additionally, an EPS matrix is produced to protect the cells from external attacks, which is the major obstacle to the penetration of antimicrobial agents.[21–23] In this way, the bacterial cells create a "bacterial-friendly" environment that protects them from antimicrobial agents. Moreover, the poor penetration efficacy is likely because these regular antimicrobial agents cannot penetrate the full depth of the biofilm.[24] It has been recognized that penetrating the bacterial biofilms is a major challenge of eliminating the dental plaque biofilm; however, disinfectants and standard antibiotics cannot work effectively due to the EPS barrier that prevents the killing of bacteria within the biofilm. Penetrating bacterial biofilms with strong anti-biofilm activity tools has recently been considered to overcome the blocking layer of periodontal tissue.[25–27] Therefore, it is critical to develop novel nanoparticles for delivering anti-bacterial agents and other therapeutics to break the EPS matrix and reach deeply into the periodontal tissue.

Several ongoing clinical trials have applied a new generation of bioparticles to increase antimicrobial activity. For instance, magnetic iron-oxide nanoparticles (MNPs) have been reported to have low cytotoxicity and good biocompatibility, whereby a magnetic field is used to take advantage of their "brute force" by pulling the MNPs to penetrate the EPS matrix.[28,29] The transfer of antimicrobial drugs by bioparticles is particularly interesting because drugs are relatively rigid and remain stable in the "brute force" delivery process. MNPs are commonly used in drug delivery and diagnostic imaging due to their simple separation procedure, magnetic properties, and low toxicity. By concentrating the magnetic field, MNPs can be immobilized close to a target, penetrate the biofilm, disrupt the EPS, and finally eliminate the biofilm. Recently, multifunctional nanoparticles have gained increased attention due to their numerous alterations and characteristics that can boost functionality, dispersibility, and stability.[30–35] However, many previously reported nanoparticles have poor permeability in periodontal pockets,[36–41] being attributed to the complex structure of the constricted and deep periodontal pocket.

Based on the above considerations, we proposed the hierarchical FPM NPs to penetrate the periodontal pockets under the magnetostatic field for treating periodontitis. Initially, Fe_3O_4 NPs were conveniently modified with PDA through the self-polymerization of dopamine in alkaline solutions. The polymer-coated nanocomposites could significantly enhance the drug loading content through electrostatic interactions with the amine-based drugs and π-π interaction force with conjugated molecules, which are also stable in the tissue fluid, facilitating their antibacterial effect at the gingival tissue. Derived from tetracycline, minocycline is considered one of the most commonly used antibiotics against Gram-negative and Gram-positive anaerobes involved in chronic periodontitis. Additionally, minocycline treatment inhibited MMPs and destroyed the periodontium constituents, such as fibronectin, proteoglycans, elastic fibers, and collagen. Hence, it was selected as a model drug owing to its amine functionality, as the active double bonds could carry out the electrostatic and π-π interactions with the guest molecule.

Here, we report that FPM NPs can overcome the dental plaque biofilm by enhancing the penetration efficacy under magnetic targeting, enabling minocycline drug delivery to deep periodontal tissue and biofilms. FPM NPs treatment also could be an ideal carrier for antibacterial drugs, as observed by the reduced colony formation of *S. sanguinis, F. nucleatum*, and *P. gingivalis*. This study reveals the importance of FPM + MF treatment for periodontitis and provides a new type of nanoparticles for treatment in Wistar rats.

Materials and Methods

Ethical Statement

The authors are accountable for ensuring that all parts of the work are appropriately investigated and resolved with accuracy and integrity. The study was conducted in accordance with the Declaration of Helsinki (Seventh revision

(2013)). The study was approved by the Ethics Committee of Nanchang University, and informed consent was obtained from all patients.

Materials

All the chemical agents were analytical reagents (AR). Iron oxide (II, III) magnetic nanoparticles solution was obtained from Aladdin Biochemical Technology Co., Ltd (Shanghai, China). Dopamine hydrochloride, Tris (hydroxymethyl) aminomethane, Tris (hydroxymethyl) aminomethane hydrochloride, and minocycline hydrochloride (Mino) were provided by Aladdin Biochemical Technology (Shanghai, China). Brain heart infusion (BHI) broth was supplied by Qingdao Hope Bio-Technology (Qingdao, China). Hemin was obtained from Hefei BASF Bio-Technology (Hefei, China). The Cell Counting Kit-8 (CCK-8) and AO/EB double stain Kit were supplied by KeyGen Biotechnology (Nanjing, China). The MTT staining kit was purchased from Solarbio Science & Technology Co., Ltd (Beijing, China). LIVE/DEAD bacterial kit was provided by Molecular Probes (Eugene, USA). The antibodies against IL-6, IL-1β, and TNF-α were sourced from Affinity Biosciences Co., Ltd (Changzhou, China).

Synthesis and Minocycline Loading of Fe_3O_4 Nanoparticles and Fe_3O_4 Magnetic Nanoparticles

The synthesis of Fe3O4@PDA nanocomposites was processed as previously described.[42] Briefly, after mixing 5 μL of Fe_3O_4 nanoparticles solution with 500 μL deionized water, the 500 μL deionized water was removed by magnet adsorption. The separated nanoparticles were dispersed again using 500 μL Tris-Buffer solution (pH = 8.5). After another dispersion using 30 mL Tris-Buffer solution, 2 mL dopamine hydrochloride solution (1 mg/mL) was added, stirred, and mixed for 1 h. Next, the supernatant was removed after fixation and adsorption using a magnetic block for 3–5 min, and the Fe_3O_4@PDA nanoparticles were resuspended using 10 mL of deionized water to remove the Tris-Buffer solution. The supernatant was removed again by adsorption for 3–5 min. Finally, the Fe_3O_4@PDA nanoparticles solution was created by suspending the Fe_3O_4@PDA nanoparticles in 500 μL deionized water.

Minocycline hydrochloride (2 mg) was added into 4 mL of deionized water and ultrasonically dispersed to prepare a 0.5 mg/mL minocycline hydrochloride solution. Then, 300 μL of minocycline hydrochloride solution and the liquid containing 0.5 mg Fe_3O_4@PDA nanoparticles were added to 10 mL of deionized water, and the mixture was stirred and mixed for 2 h. The black precipitate was obtained after fixation and adsorption with a magnetic block for 3–5 min, followed by removing the supernatant. Subsequently, 500 μL of deionized water was added to obtain the Fe_3O_4 @PDA@Mino nanoparticle solution. The drug loading rate was calculated by measuring the absorbance of minocycline hydrochloride at λ = 348 nm using a UV spectrophotometer.

Characterization of Different Nanoparticles

The size and shape of nanoparticles were characterized using transmission electron microscopy (TEM, Talos F200X, FEI, US) and Scanning Electron Microscopy (SEM, Regulus 8100, Hitachi, Japan). The hydrodynamic diameters and the charge of nanoparticles were measured by Nano Sizer and Zeta-potential Tester (NanoBrook Omni, Brookhaven, US). The thermogravimetric analysis (TGA) was performed on a thermogravimetric Analyzer (Discovery TGA55612-1, USA) with a heating rate of 5 °C/min. The magnetic property of the samples was investigated at room temperature by a vibrating sample magnetometer (VSM) (model 7404, Lake Shore, USA).

The Examination of Drug Release in vitro

FPM magnetic nanoparticle liquid was added to the dialysis bag, sealed on the top and bottom with dialysis bag clips, added to a 50 mL centrifuge tube with built-in 29 mL PBS buffer solution, and placed in a flat rocking shaker at 200 rpm and maintained at a constant temperature of 37°C. While oscillating, 3 mL of the solution was taken at regular intervals and mixed with 3 mL of fresh PBS solution to measure the absorbance at 800 nm using a UV-Vis spectrophotometer. The minocycline drug loading of FPM in the solution was calculated at each time point from the pre-measured working curve

y = 0.0316x + 0.0003. The drug release rate and the drug release curve of the drug-loaded particles in the buffer solution at different time points can be calculated using the following formulas;

$$\text{Drug release rate}(\%) = (\text{amount of drug in solution}/\text{total drug loading of drug} - \text{loaded particles at aspecific time point}) \times 100\%$$

$$\text{Drug loading}(\%) = (\text{drug mass in the carrier}/\text{total mass of the nanocarrier}) \times 100\%$$

$$\text{Encapsulation efficiency}(\%) = (\text{the mass of the drug in the carrier}/\text{total mass of drug added}) \times 100\%$$

In vitro Biocompatibility Evaluation of Fe_3O_4@PDA

L929 Cell Line Culture

The L929 cells (National Collection of Authenticated Cell Culture, Shanghai, China) were cultured in DMEM containing 10% FBS and 1% penicillin/streptomycin. After 24-hour incubation in a 96-well plate, the L929 cells were attached to the bottom of the well. The Fe_3O_4 NPs and Fe_3O_4@PDA NPs were diluted into suspensions of 20 μM, 50 μM, 0.1 mM, and 0.2 mM. The original medium in each well was discarded, and the cells were incubated in different nanoparticle concentrations according to the experimental design for 24 hours. The same amount of fresh medium was used as a control. After 24-hour culture, CCK-8 solution (10 μL/well) was added into the wells, followed by incubation in a constant temperature incubator for 2 h. The absorbance value (OD) was then measured at a wavelength of 450 nm using a microplate reader (Infinite 200 Pro, Tecan, Austria). The formula used for calculating cell viability was:

$$\text{Cell viability rate}(\%) = (\text{OD treated} - \text{OD blank}) \times 100\% / (\text{OD control} - \text{OD blank})$$

$$\text{Cell viability rate}(\%) = \frac{\text{OD treated} - \text{OD blank}}{\text{OD control} - \text{OD blank}} \times 100\%$$

Where OD treated, blank, and control represent the OD values of treated, blank, and negative control groups, respectively.

Cellular Biocompatibility Assay

The L929 cell suspension (1 mL/well) in the logarithmic growth phase was seeded in a 24-well plate at a density of 6×10^4/well and cultured in a constant temperature incubator for 24 hours. After the cells were attached to the bottom, different concentrations of nanoparticle suspensions of various concentrations were added to the experimental groups and incubated for 24 hours, whereas the same amount of fresh medium was added to the control cells. The liquid in the plate was discarded, followed by washing twice with PBS. Then, 500 μL staining solution, 5 μL acridine orange (AO), and 5 μL ethidium bromide (EB) staining solution was added to the resuspended cells. Finally, the cells were incubated in the dark for 3 minutes after gentle mixing. After washing with PBS, the cell number and morphology were measured using a fluorescence microscope (DMi8, Leica, Germany), and the LIVE/DEAD staining assay was performed.

In vitro Assessment of Antibacterial Properties

Bacterial Strains Culture

The bacteria used in this study, such as *S. sanguinis* (ATCC 10556), *P. gingivalis* (ATCC 33277), *and F. nucleatum* (ATCC 10953), were provided by the American Type Culture Collection (ATCC, Manassas, VA, USA). The usage and protocols of the bacteria-related experiments were approved by the Institutional Review Board of Nanchang University, School of Dentistry. BHI containing Vitamin K (1 mg/L) and hemin (5 mg/L) was used for bacterial culture. *P. gingivalis* and *F. nucleatum* were incubated under anaerobic conditions, whereby palladium pellets were dried at high temperatures and treated with 1.3 g citric acid, 1.3 g sodium bicarbonate, 1.1 g potassium borohydride, and water in an anaerobic box. *S. sanguinis* was incubated in an aerobic incubator at 37°C. Using the turbidimetric method, the bacterial concentration was adjusted to 10^9 colony-forming units (CFU) per mL for subsequent single-strain biofilm formation and antibacterial experiments.

CFU Counts for Planktonic Bacteria After Different Treatments

The bacteria were recovered and passaged for two consecutive days, then diluted to 10^8 CFU/mL. The three bacterial strains were cultured with 5 treatments at a 1:1 ratio for 6 hours: control, Mino, Fe_3O_4 NPs, Fe_3O_4@PDA NPs, and FPM NPs. Finally, the bacterial suspension from each group was serially diluted and evenly spread onto the BHI agar plates. After 24-hour culture at 37 °C, a colony counter (Reichert Inc., USA) was employed for calculating the CFU. Three replicates were performed for each bacteria-treatment group.

Formation of Single-Species Biofilm on Hydroxyapatite Disk

For saliva sample collection, volunteers were recruited with natural dentition, no oral bacterial diseases such as active dental caries, and no antibiotics in the last 3 months. Volunteers were requested not to brush their teeth for 24 hours and avoid eating for 2 hours before saliva collection. Equal amounts of saliva from 15 healthy volunteers were mixed to get the saliva samples, followed by centrifugation (3000 rpm, 20 min) to get rid of cellular debris. Subsequently, the supernatant was filtered by a bacterial filter (0.22 μm). To simulate the intraoral environment, hydroxyapatite disks (diameter 5 mm) were soaked in saliva and pretreated at 37°C for 2 hours to form a saliva film on the hydroxyapatite discs.

Establishment of a single-strain biofilm: Under sterile conditions, the hydroxyapatite discs wrapped with the saliva film were placed at the bottom of a 24-well plate and treated with *S. sanguinis, P. gingivalis*, or *F. nucleatum* at 10^8 CFU/mL. Then, 10 μL/mL were inoculated onto hydroxyapatite sheets. After 10 min of bacterial suspension, 1 mL of culture medium was added, and the medium was changed regularly every day. A biofilm would be formed in about 4 days. Five experimental groups were set for the following experiment:

1. Blank control group: PBS
2. Negative control group: 10μL (20 μg/mL) Fe_3O_4 NPs
3. Positive control group: 10μL (20 μg/mL) minocycline
4. Experimental group: 10μL (20 μg/mL) Fe_3O_4@PDA NPs
5. Experimental group: 10μL (20 μg/mL) Fe_3O_4@PDA@Mino NPs (referred to as FPM group)

Magnetic-Targeting FPM NPs Penetrate Periodontal Biofilm on Hydroxyapatite Disk

After 4 days of *P. gingivalis* biofilm growth on the hydroxyapatite disk, the medium was removed, and the disk was washed with 1 mL PBS. Then, 10 μL FPM NPs suspension (20 μg/mL) was placed on the biofilm in each well. A NdFeB magnet (50×30×10 mm, 2000–2200 Gs surface magnetic field intensity) was placed at the bottom of the well for 5 min to magnetically drive the FPM NPs to penetrate the biofilm surface.

CFU Counts, Metabolic Activity, and LIVE/DEAD Fluorescent Staining for Single-Species Biofilms on the Hydroxyapatite Disk

The biofilm on the hydroxyapatite disk was scraped off with a scalpel, rinsed twice with 1 mL of PBS in a 24-well plate, transferred to a 1.5 mL EP tube together with the hydroxyapatite disk, then sonicated (KQ-400DE, Kunshan Ultrasonic Instrument, China) and vortexed (Vortex-6, Kylin-Bell, China) for 20 min to disperse the bacteria. The obtained bacterial suspension was gradually diluted in multiples of 10 with bacterial culture medium, then a drop (10 μL) of the diluted bacterial suspension was spread onto a BHI agar plate. Finally, the number of colonies was counted to calculate CFU with the dilution factor. Each experiment was repeated three times.

MTT assay was carried out to evaluate the metabolic activity in the biofilm's bacteria. The biofilm-adhered hydroxyapatite disks were PBS-rinsed to remove unattached biofilm. The hydroxyapatite disks were then transferred into a 24-well plate. After that, the MTT staining solution (1 mL) was added to each sample, followed by incubation for 1 h at 37°C. Next, the blue-violet crystalline formazan was dissolved using the same amount of dimethyl sulfoxide (DMSO). After 20-minute shaking horizontally in the dark, the DMSO solution was transferred to a 96-well plate, and the OD of each well was measured at 540 nm using a microplate reader.

Treated bacteria were stained using SYTO9 (0.25 μM) /propidium iodide (0.25 μM) to determine the LIVE/DEAD status. A confocal laser scanning microscope (CLSM) (A1 HD25, Nikon) was employed to record the dead (Red color) and live (Green color) bacteria.

In vivo Assessment of Antibacterial Properties

Animal Model Construction and Nanomedicine Administration

All animal-related procedures complied with the Guidelines for the Care and Use of Laboratory Animals of Nanchang University in China and were approved by the Animal Ethics Committee of ZHBY Biotech Co. Ltd (Document No. 2021121301). Male Wistar rats aged 4–6 months were provided by Zhejiang Weitong Lihua Laboratory Animal Technology. All the rats were kept in a humidity- and temperature-constant environment at a light-dark cycle of 12h:12h. The rats accessed Ad libitum food and water during all the experiments. The rats were assigned randomly to the following 5 groups:

1. Blank control group (Control)
2. Periodontitis model group (Periodontitis)
3. Periodontitis model + minocycline group (referred to as Mino group)
4. Periodontitis model + FPM NPs + magnetic field (referred as FPM+MF group)
5. Periodontitis model + FPM NPs (referred to as FPM group)

After treatment with antibiotics for 3 days, rats were intraperitoneally injected with chloral hydrate (10%, 0.3 mL/100 g) for anesthetization. Subsequently, a bacterial-induced periodontal inflammation model was established as follows: after anesthesia, orthodontic ligation and suture silk thread are ligated to the mandibular first molar of the rat, placed under the gum, and knotted on the lingual side. Twenty μL of the mixed bacteria solution (*F. nucleatum, P. gingivalis*, and *S. sanguinis*, 1:1:1, 10^8 CFU/mL) was injected continually for 7 days into the gingival sulcus, and a periodontitis model was established using a high-sugar and high-viscosity diet combined with a bacterial smear method.

After successful modeling, the ligation wire was removed, and 50 μL of the corresponding drug (20 μg/mL) solution was locally injected into the periodontal pocket for 5 consecutive days. The head of the rats in the FPM + MF group was placed above the magnet (embedded in a 100×50×20 mm foam board, with a 3200–3500 Gs surface magnetic field intensity) after drug injection, and the magnetic targeting state was maintained for 15 minutes (supine, and left and right lateral decubitus positions for 5 minutes each). Twenty-four hours after the administration, the rats were sacrificed by abdominal aortic bloodletting after intraperitoneal anesthesia. The buccal and lingual gums of the maxillary first molars and the alveolar bone around the maxillary first molars of the rats in each group were collected, followed by normal-saline washing and paraformaldehyde (4%) fixation. In addition, the kidneys, lungs, spleen, liver, and heart were taken. The formalin-soaked and paraffin-embedded sections were stained with HE.

Histomorphometry Analyses

After 2 hours of washing with running water, the tissues were dehydrated by successive incubation in 70%, 80%, 90%, and 100% alcohol solutions for 15 min. Then, the tissues were cleared by subsequent incubation with xylene and 100% alcohol solution for 15 min, xylene I for 15 min, and xylene II for another 15 min. After a 15-minute fixation with the xylene/paraffin mixture and incubation in paraffin I and paraffin II permeation solutions separately, the tissues were embedded and cut into 5 μm thick sections. The sections were stained with Hematoxylin aqueous solution for 3 minutes, then in a hydrochloric acid/alcohol solution for 15 seconds. After That, sections were washed with running water, stained with the blue solution for 15 seconds, and rinsed with running water. The sections were then stained with eosin for 3 minutes and sealed with mounting medium. A semi-quantitative scoring system was applied to review and score the slides blindly.

Quantitative Real-Time PCR (qRT-PCR) and Western Blotting Analyses

For each group, total RNA extraction from the gingival tissues was carried out, followed by cDNA synthesis using a reverse transcription kit. The cDNA was used as a template for quantitative fluorescence PCR. The relative expression levels of IL-1β, IL-6, and TNF-α in gingival tissue cells of each group were quantified by qRT-PCR. Primer information, operating system, and reaction procedures are listed in Table 1–3.

Table 1 Primer Sequences

Primer	Sequence (5'-3')
β-actin F	GCCATGTACGTAGCCATCCA
β-actin R	GAACCGCTCATTGCCGATAG
IL-1β F	CAGACCCCAAAAGATTAAGGATTG
IL-1β R	CTAGCAGGTCGTCATCATCC
IL-6 F	CTTCTTGGGACTGATGTTGTTG
IL-6 R	GACTCTGGCTTTGTCTTTCTTGTTA
TNF-α F	CAACAAGGAGGAGAAGTTCCCAAAT
TNF-α R	GCTTGGTGGTTTGCTACGA

Table 2 qRT-PCR Reaction System

Reagents	Volume (20μL Total)
2 × ChamQ Universal SYBR qPCR Master Mix	10μL
cDNA	1μL
Primer F	0.4μL
Primer R	0.4μL
RNase Free ddH_2O	8.2μL

Table 3 qRT-PCR Reaction Program

Steps	Temperature	Time	Cycles
Pre-denaturation	95°C	10min	1
Denaturation	95°C	10s	40
Annealing	58°C	30s	40
Elongation	72°C	30s	40

Total protein was extracted from the cells of each group with ice-cold cell lysis buffer. The homogenates were placed on ice for 30 min, then centrifuged at 10,000 rpm/min for 10 min at 4°C, followed by the aspiration of the supernatant to obtain total protein. The quantification of protein concentration was conducted using the PierceTM BCA Protein Assay kit. The protein sample (20 μg) was denatured, loaded, and ran on SDS-PAGE for 1–2 hours, then transferred to a polyvinylidene fluoride (PVDF) membrane. Following 1-hour incubation in a 5% blocking solution, the membrane was incubated with primary antibodies overnight at 4°C, then washed and incubated for 1–2 hours at room temperature in the secondary antibody solution. The visualization of Blots was performed using an ECL solution, followed by imaging in a gel imaging system. Finally, the bands were analyzed using "Image J" software.

Statistical Analysis

Statistical analysis was conducted using SPSS. Comparisons among groups were performed using one-way analysis of variance (ANOVA) test. Results are presented as mean ± standard deviation (SD). Differences with a p-value < 0.05 were statistically significant.

Results

Characterization of Polydopamine-Modified Iron Oxide Nanoparticles

We synthesized the polydopamine-modified iron tetroxide nanoparticles (Fe_3O_4@PDA NPs) using a simple co-precipitation method.[42] The reaction between iron oxide nanoparticles and polydopamine was tested for 0.5, 1, and 2 hours (Table S1). Based on the potential and particle size, the 1-hour reaction was selected for subsequent experiments.

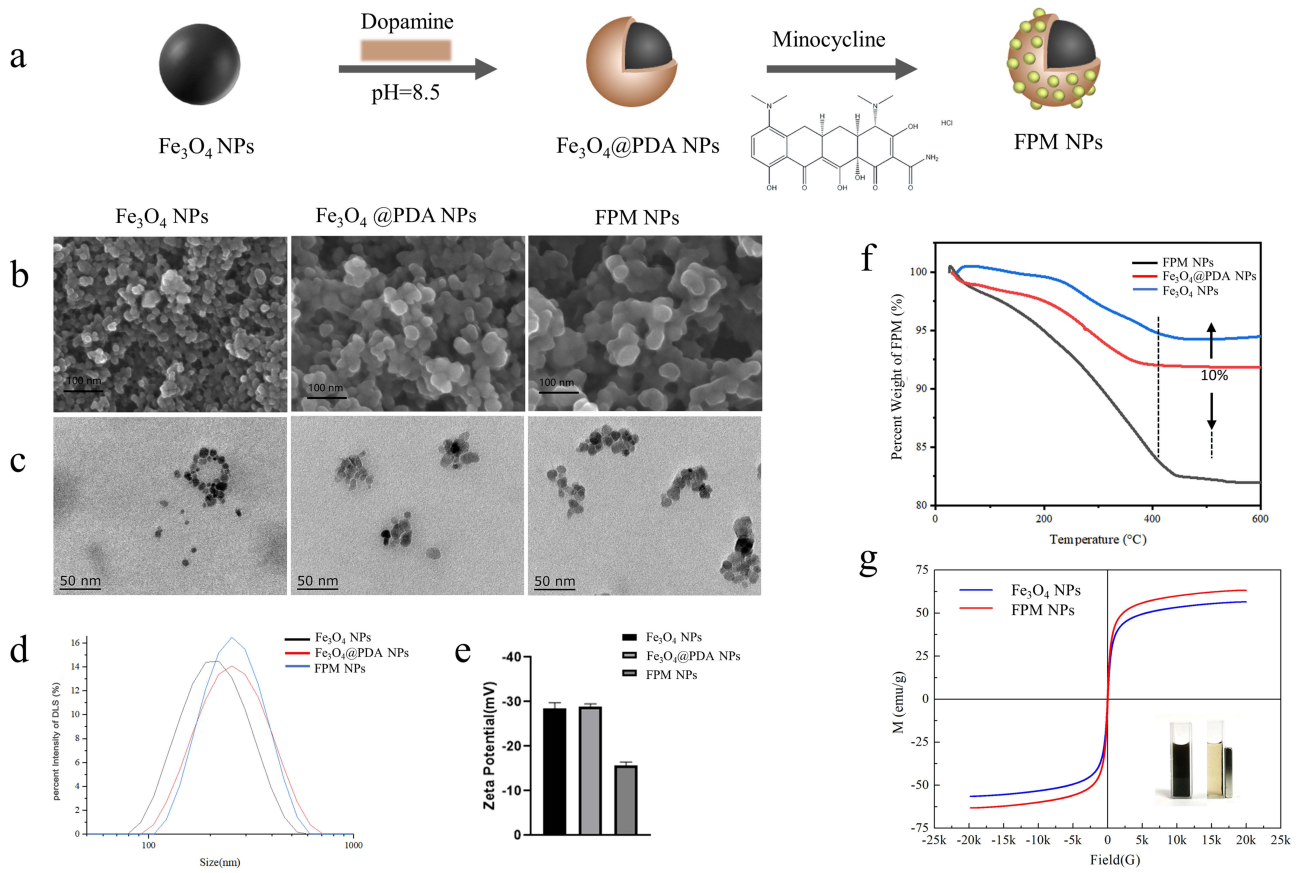

Figure 1 The synthesis and characterization of Fe_3O_4 NPs, Fe_3O_4 @PDA NPs, and FPM NPs. (**a**) A schematic illustration of FPM NPs synthesis. (**b** and **c**) SEM and TEM images of Fe_3O_4 NPs, Fe_3O_4 @PDA NPs, and FPM NPs. (**d**) Representative images showing the diameter distribution of the PBS-suspended magnetic nanoparticles. (**e**) Zeta potentials of magnetic nanoparticles in water (pH 7.0). (**f**) Thermogravimetric analysis of Fe_3O_4 NPs, Fe_3O_4 @PDA NPs, and FPM NPs. (**g**) Magnetic hysteresis loops at 300 K for Fe_3O_4 NPs and FPM. The inset in the lower right corner displays FPM's magnetic behavior under an applied external magnetic field.

A simple co-precipitation method was applied to load the polydopamine-modified iron oxide nanoparticles with minocycline (Figure 1a). The morphological attributes of diverse nanoparticles obtained using TEM and SEM are shown in Figure 1b. The SEM images of Fe_3O_4 NPs showed spherical structures. No change of the Fe_3O_4@PDA NPs morphology was observed after coating by the self-polymerization of dopamine to polydopamine. TEM images showed a thinner polymer shell around the dopamine hydrochloride and minocycline-coated Fe_3O_4 NPs, which cannot be detected on the uncoated nanoparticles. Besides, the spherical and well-dispersed features without agglomeration indicate a good mono-dispersity of the particle (Figure 1c). DLS (Dynamic Light Scattering) was conducted to obtain the size distributions of the Fe_3O_4 NPs, Fe_3O_4@PDA NPs, and FPM NPs. Figure 1d shows that the particle size increased with the coating of PDA, and the zeta potential decreased with Mino loading. The results of the DLS analysis also showed that the average diameters of Fe_3O_4 NPs, Fe_3O_4@PDA NPs, and FPM NPs were 217.6 nm, 270.6 nm, and 273.7 nm, respectively (Figure 1c). The gradual increase in diameters may be partially caused by the modification layer-by-layer from Fe_3O_4 NPs to FPM NPs. The zeta potential of Fe_3O_4 NPs is approximately −15 mV (Figure 1d). These particles absorbed light at 400 nm, and the thermogravimetric analysis showed that the loss ratio of FPM NPs is about 10% lower than the Fe_3O_4@PDA nanoparticles, indicating a relative drug loading rate of 10% (Figure 1e). As shown in Figure 1F, the magnetization curves of the FPM NPs powder samples were measured at room temperature with an applied magnetic field ranging from −25k to +25k Oe. When the magnetic field is removed, both the Fe_3O_4 and polymer Fe_3O_4 nanoparticles exhibit negligible coercivity and remanence, implying that the magnetic nanoparticles are paramagnetic, possessing FPM's magnetic behavior under an external magnetic field.

A prominent attribute of coating the shell with PDA is the improved drug loading and encapsulation efficiency through the electrostatic and π-π interactions with the guest molecule. The drug loading and encapsulation efficiency of FPM NPs were 9.0 ± 1.0% and 33.1 ± 4.1%. To evaluate the quality of our designed nanoplatforms, the release rate and degree of Mino were measured by the dialysis bag dissolution method to mimic the drug-local physiological environment. Mino from FPM NPs was quickly released into PBS (pH 7.4) in the first 12 hours, then slowly released for a week to about 8% (Figure S1). This generally includes the secondary release of the drug to maintain the efficient concentration of antibiotics. The increased concentration of antibiotics after the full release favored bacterial killing at periodontal pockets.

In vitro Biocompatibility Evaluation

To verify the biocompatibility of our synthesized nanoparticles, L929 cells were treated with concentrations of 20 μM, 50 μM, 100μM, and 200 μM each of Fe_3O_4 NPs, Fe_3O_4 @PDA NPs suspension solutions. The CCK-8 kit showed that the cell viability is greater than 90% when the concentration is 0–50 μg/mL (Figure 2a). LIVE/DEAD staining showed that a large number of live bacteria were still present at concentrations between 20–200 μg/mL, indicating good biocompatibility (Figure 2b).

In vitro Antibacterial Evaluation

Effects of FPM NPs on Periodontal-Associated Planktonic Bacteria

Due to their potent effect on the occurrence and development of periodontitis,[43] *P. gingivalis, F. nucleatum*, and *S. sanguinis* were used to evaluate the antibacterial activity of our fabricated nanocomposites in vitro. The anti-planktonic-bacterial capability of the designed nanocomposites was determined by the colony counting method before analyzing the anti-biofilm results. Figure 3a presents plate counts photographs of three periodontal-associated planktonic bacteria. As evident, FPM exhibited the best antibacterial effect, decreasing colony formation of *S. sanguinis, F. nucleatum*, and *P. gingivalis* compared to the control group, with antibacterial effects similar to minocycline (Figure 3a). The bacterial CFU results of *S. sanguinis, F. nucleatum*, and *P. gingivalis* showed that Fe_3O_4 and Fe_3O_4 @PDA had similar effects as the control. However, FPM exhibited the highest antibacterial effect, where it inhibited the growth of the bacteria significantly compared to the control group, reaching a level similar to minocycline (Figure 3b).

Anti-Biofilm Efficacy of FPM NPs on Periodontal-Associated Bacterial Biofilms

Single-strain biofilms were established and used to detect the penetrating efficacy of FPM NPs and their effect on the microscopic morphology and architecture of the biofilms after magnetic impulse (Figure 4a). The colony formation of *S. sanguinis, F. nucleatum*, and *P. gingivalis* is shown in Figure 4b. The summarized results of CFUs showed that FPM has a similar sterilization effect as minocycline ($p>0.05$), while FPM + MF (magnetic field) has a pronounced killing effect on three periodontal-associated bacterial biofilms. The antibacterial effect of FPM with a magnetic field was significantly increased compared with that of FPM alone ($p<0.01$), indicating that FPM NPs could penetrate the deep

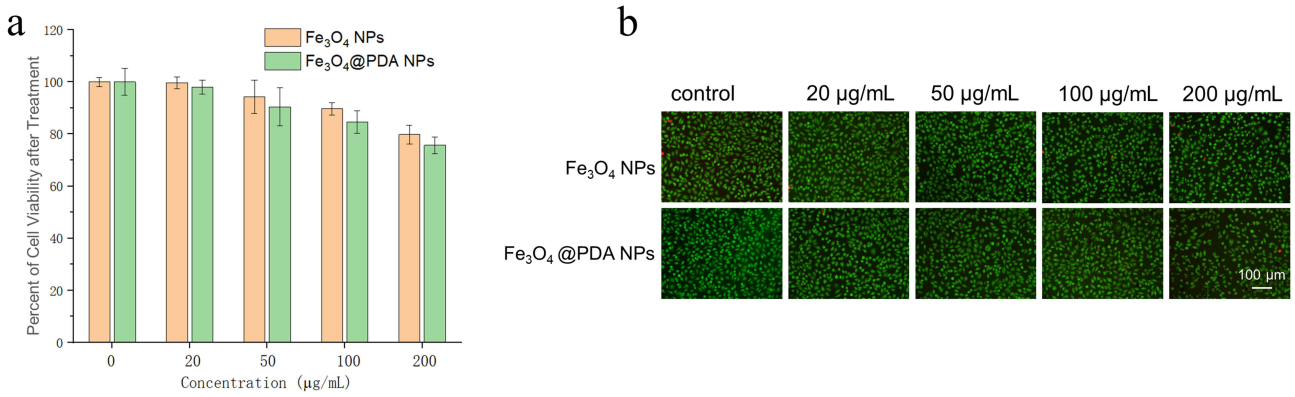

Figure 2 (**a**) Cell viability rate and (**b**) AO/EB stain of L929 cells after treatment with Fe_3O_4 NPs and Fe_3O_4 @PDA NPs for 24 h.

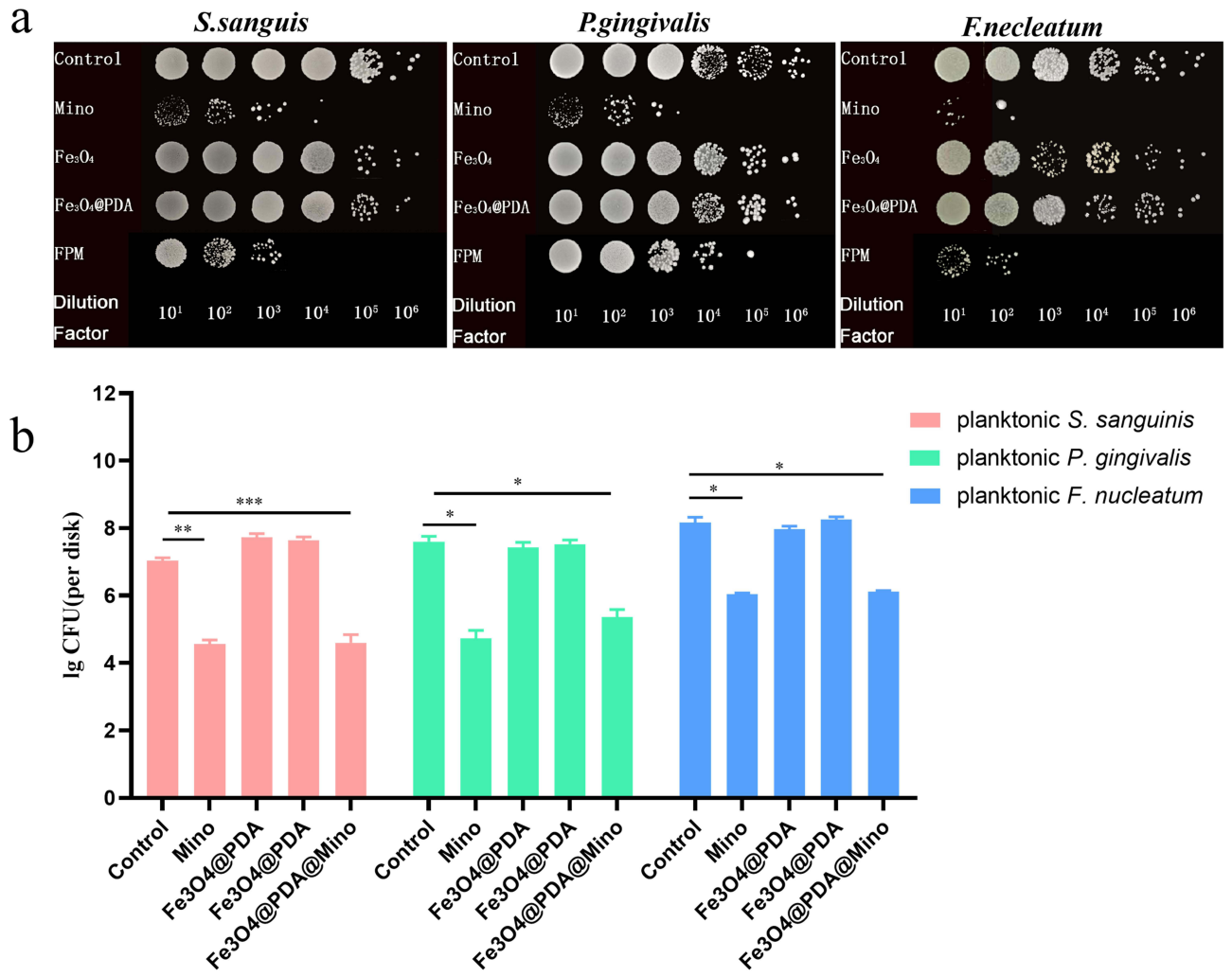

Figure 3 The antibacterial effect of FPM against planktonic bacteria. (**a**) Representative images showing the colony formation of planktonic *S. Sanguis, (P) gingivalis, and F. nucleatum*. (**b**) A bar graph showing the CFU of planktonic *S. Sanguis, (P) gingivalis*, and *F. nucleatum* after indicated treatments. (Student's *t*-test, *, $p < 0.05$, **, $p < 0.01$, ***, $p<0.001$).

layer of biofilms and enhance antibacterial efficacy under magnetic impulse. We also observed the lowest metabolic activity after treatment with FPM + MF (Figure 4c).

To further confirm the antibacterial effect of FPM with the magnetic field, we used the fluorescence LIVE/DEAD dye to label the bacteria in *P. gingivalis* biofilms after different treatments. Under CLSM, green fluorescence indicates live bacteria, and red indicates dead bacteria (Figure 5a). As shown in the merged and 3D CLSM images in Figure 5a, we observed complete live bacteria in the Positive Control and substantial amounts of dead bacteria in the Mino groups. The pure FPM-treated group showed a similar percentage of live and dead bacteria. More dead and fewer live bacteria were observed in the FPM + MF group compared to the other treatments, suggesting the most potent antibacterial property against the periodontal biofilm. The result of live/dead staining for periodontal biofilm was consistent with the conclusion obtained by quantification of CFUs.

SYTO and CLSM images of stained *P. gingivalis* biofilms were taken to test our hypothesis that FPM NPs can be driven into the biofilms and disrupt the EPS's integrity to promote antimicrobial penetration and killing bacteria by antimicrobials under a magnetic field. The untreated *P. gingivalis* biofilm appeared highly compact in a transverse cross-sectional image before magnetically forcing FPM NPs to move through it (Figure 5b). The integrity of the biofilm was disrupted, and its thickness decreased after magnetically directing FPM NPs to move through the biofilm (Figure 5b). These data demonstrate that magnetic impulses could pull FMP NPs against the biofilm mass and kill bacteria deep within it.

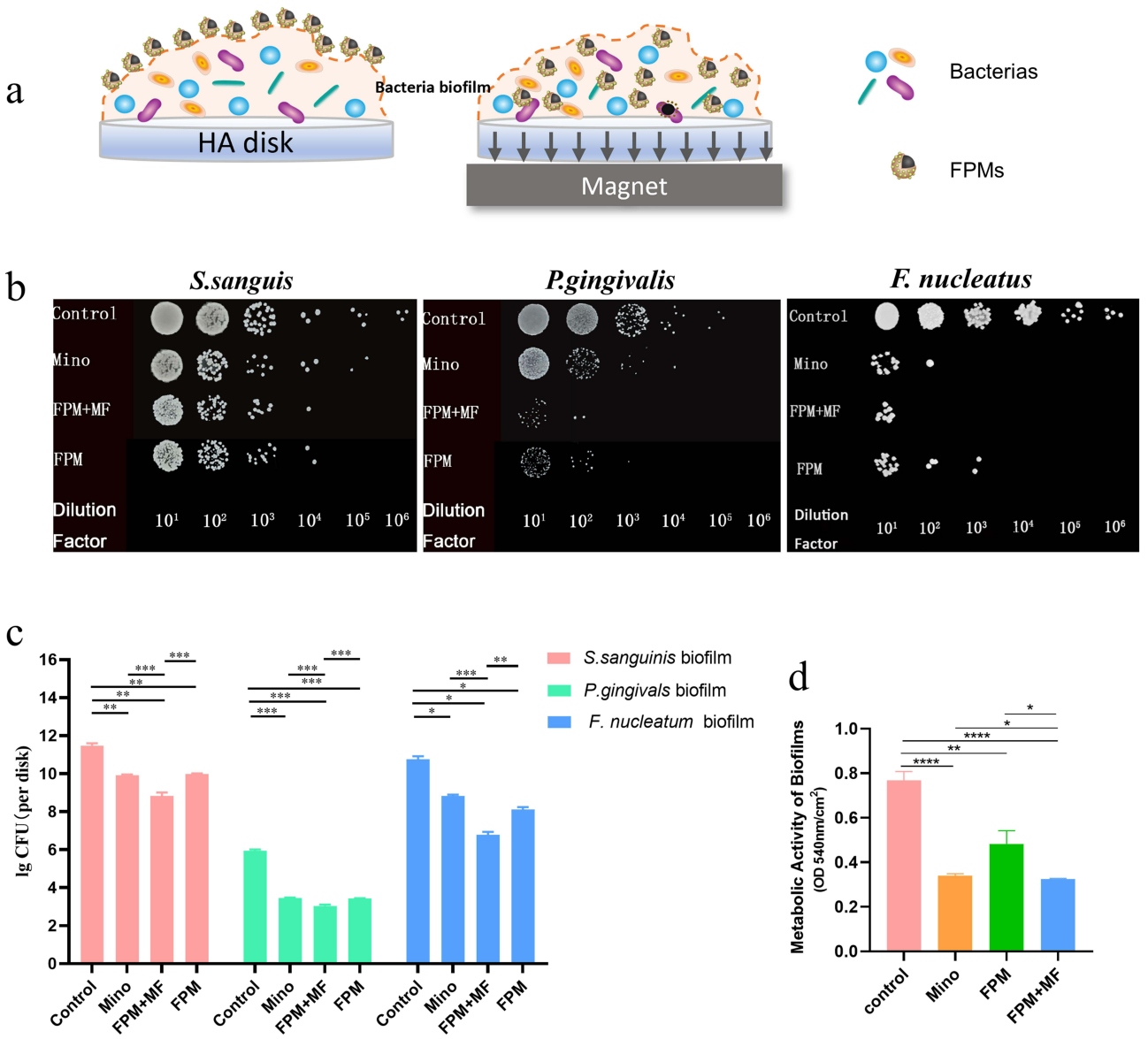

Figure 4 The antibacterial effect of FPM against biofilm. (**a**) A schematic representation of FPM NPs penetration into biofilm on HA disk under the motivation of magnetic field. (**b**) Representative images showing the colony formation of planktonic *S. Sanguis, (P) gingivalis*, and *F. nucleatum*. (**c**) A bar graph showing the CFU of planktonic *S. Sanguis, (P) gingivalis*, and *F. nucleatum* after different treatments. (**d**) A bar graph showing the metabolic activity of *P. gingivalis* biofilms after different treatments. (Student's *t*-test, *, $p < 0.05$, **, $p < 0.01$, ***, $p<0.001$, ****, $p<0.0001$).

Antibacterial Evaluation in vivo

Animal Periodontitis Model and Nanomedicine Administration

To explore the effect of magnetic nano-drug carriers on periodontitis, we established a bacterial-induced periodontal inflammation model in male Wistar rats (Figure 6a). After treatment with different nanoparticles for 5 days, the pathological changes were examined by HE staining. The rats in the periodontitis group displayed dark red gingiva, with noticeable swelling, mucosal erosion at the gingival margin, and heavy bleeding on probing. On the other hand, the gingival tissues of rats in the Mino and FPM groups were slightly red and brittle, with minor bleeding. The gingiva of rats in the FPM + MF group was pink, rigid, and elastic, without bleeding on probing (Figure 6b).

HE staining images showed that the gingival tissue of rats in the periodontitis group had dramatically increased diffuse inflammatory cells such as monocytes, macrophages, neutrophils, and lymphocytes compared to the control

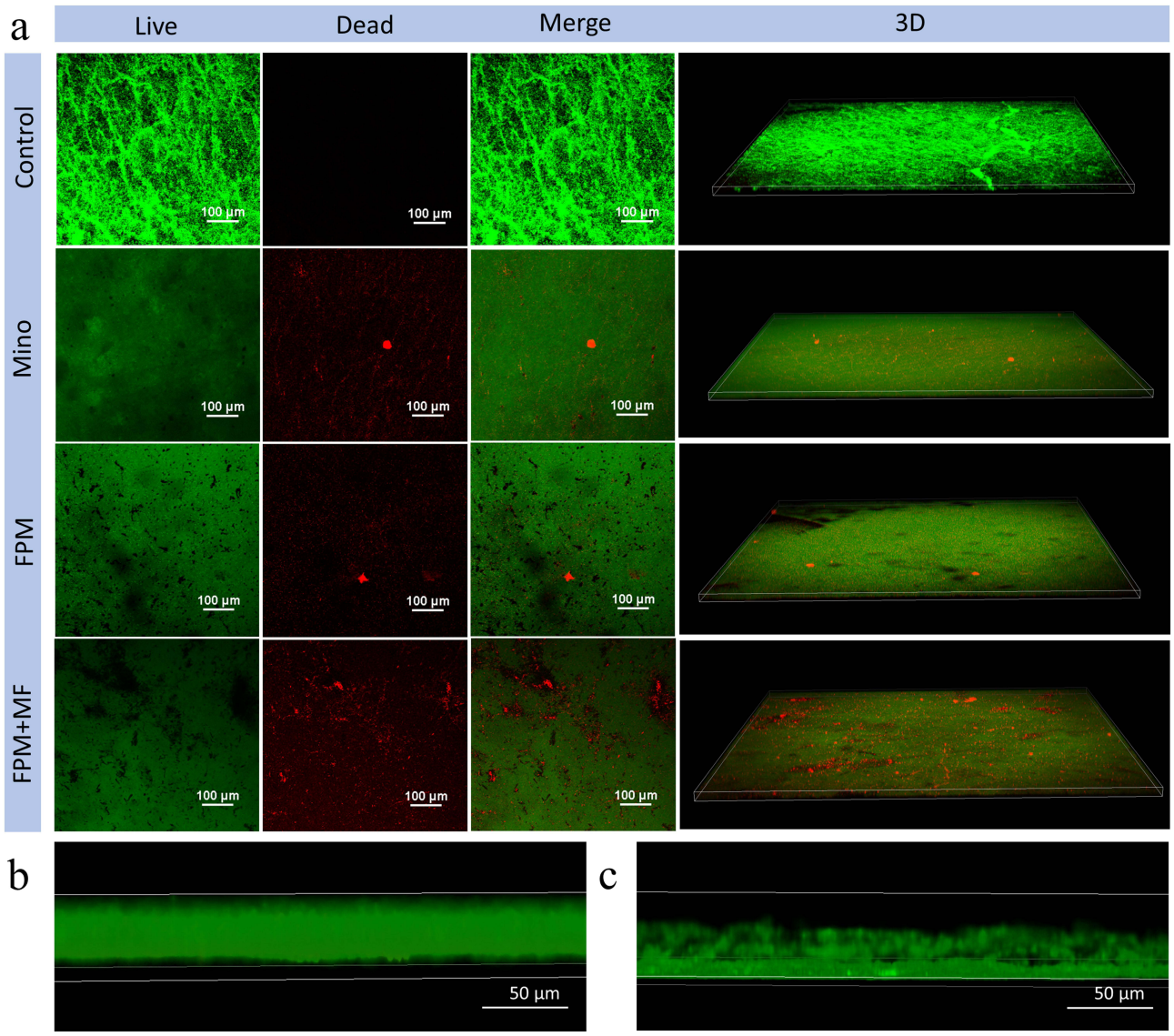

Figure 5 CLSM images of periodontal biofilms after different treatments. (**a**) Representative live/dead and 3D reconstruction images of *P. gingivalis* on HA disks (dead bacteria stained red; live bacteria stained green). (**b** and **c**) Penetrating effect of FPM on biofilms. Transverse cross-sectional CLSM images of periodontal biofilms treated with FPM before and after magnetic motivation.

group. Conversely, a small amount of infiltrated immune cells were observed in Mino and FPM groups. Interestingly, no inflammatory cell infiltration was observed in the FPM + MF group, like the control group (Figures 6c and d).

The Magnetic Targeting and Anti-Inflammatory Effects of FPM NPs on the Rat Model

Periodontitis has been linked to increased inflammation via the enhanced expression of pro-inflammatory cytokines. To further assess the anti-inflammatory effect of FPM NPs on our rat model, we conducted qRT-PCR and Western blot to analyze the expression levels of TNF-α, IL-6, and IL-1β.

Compared to the control group, IL-1β, IL-6, and TNF-α were upregulated in the periodontitis group (Figures 6e, f and g, 2nd column). After minocycline treatment, the expression levels of IL-1β, IL-6, and TNF-α were reduced compared to the periodontitis group (Figures 6e, f and g, 3rd column). The expression of IL-1β, IL-6, and TNF-α further decreased with FPM and MF combination, significantly lower than the periodontitis and minocycline groups, and even lower than the control group (Figures 6e, f and g, 4th column). Interestingly, the FPM solo treatment could not down-regulate these pro-inflammatory genes

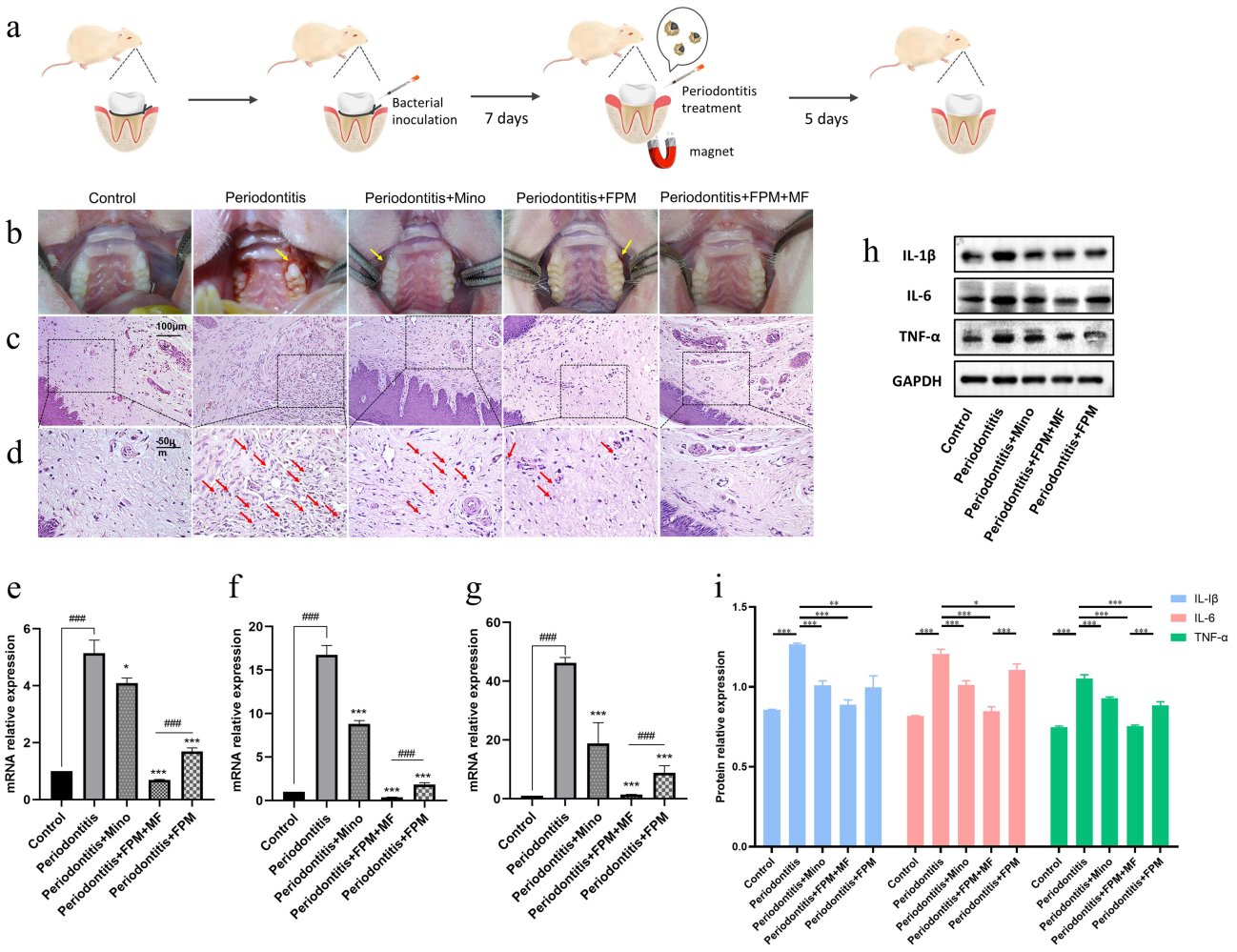

Figure 6 In vivo therapeutic assessment of periodontal inflammation in rat models after treatment. (**a**) Schematic diagram of the in vivo experiments, including the animal model and local treatment with FPM NPs under magnetic motivation. (**b**) Intraoral images of model rats after treatment using different nanoparticles. The yellow arrows indicate inflammatory symptoms such as gingival redness, swelling, and bleeding. (**c** and **d**) Representative images of periodontal H&E staining from rats after local application of different treatment strategies. The immune cells, such as lymphocytes, neutrophils, macrophages, and monocytes, are indicated by red arrows in (d). (**e, f**, and **g**) The relative mRNA levels of pro-inflammatory genes after different treatments. (**h** and **i**) The level of pro-inflammatory proteins after different treatments. (Student's *t*-test, *, $p < 0.05$, **, $p < 0.01$, ***, $p<0.001$ compared with the periodontitis group, ###, $p<0.001$ compared with the inter-group comparison).

(Figures 6e, f and g, 5th column), indicating that FPM and MF combo treatment is the top suppressor of the pro-inflammatory genes.

Western blot data showed a similar pattern to qRT-PCR. Compared to the control group, the protein levels of IL-1β, IL-6, and TNF-α were upregulated in the periodontitis group, and the treatment of Mino, FPM, and FPM + MF suppressed their expression. The FPM+MF treatment showed the best antibiotic efficiency, suggesting that the FPM + MF treatment is an effective method for treating clinical periodontitis (Figure 6h).

Increased body weight was observed during the entire 5-day period. Additionally, hematoxylin and eosin (H&E) staining of the kidneys, lungs, spleen, liver, and heart was performed to determine any signs of metastasis or cell death. Normal and intact tissue structures were observed, and no inflammation was found in all groups (Figure S2).

Discussion

Nanoparticle-based drug delivery systems have shown great potential for treating periodontitis, a common chronic inflammatory disease affecting the tooth-supporting structures. Periodontitis can lead to tooth loss and has been linked to other systemic diseases, including cardiovascular diseases and diabetes. Traditional treatments, such as scaling and root planning, may not be sufficient to eliminate the infection, particularly in severe cases. Given the diverse biochemical

composition of bacterial plaques, previous studies focused on developing new drugs and identifying mechanisms to inhibit bacterial plaque formation. In this study, we highlighted the contribution of the FMP NPs in infiltrating bacterial plaque. Compared to traditional nanoparticle treatments, our results showed that, directed by magnetic forces, FMP NPs could successfully break through the biofilm mass and kill bacteria deep in periodontal tissue. Additionally, targeted with magnetic power, our FMP NPs showed more effective drug delivery in vivo, allowing penetration deep into the periodontal tissues, accessing hard-to-reach bacterial sites, and reducing bacterial load and inflammation in the affected area.

Several nanoparticle drug delivery systems have been investigated for periodontitis treatment, including liposomes, polymeric nanoparticles, inorganic nanoparticles, and hydrogels. These systems have shown promising results in preclinical studies, with improved treatment outcomes compared to conventional therapies. However, some challenges exist in translating nanoparticle-based drug delivery systems for periodontitis treatment into clinical practice. These challenges include potential toxicity, manufacturing scale-up, regulatory approval, and cost-effectiveness. Further research and development are required to address these issues and make such innovative treatments available to patients with periodontitis. Our in vitro study confirmed that FPM + MF treatment could be promising for a clinical trial to treat periodontitis in deep periodontal tissue.

Recent studies have shown that periodontal disease (gum disease) is a chronic inflammatory oral disease that progressively destroys the tooth-supporting apparatus.[44,45] Generally, regular cleaning could eliminate bacterial plaque. However, bacterial plaque deep in the periodontal pocket will be challenging to remove if the periodontal disease progresses. Additional treatments like scaling and root planing, antibiotics, or surgical intervention may be required to control the disease and prevent further damage to the periodontal tissues. Periodontal treatment aims to break the pathogenic bacterial biofilm and deliver antibacterial drugs to suppress bacterial infection.[46,47] Most of the previously developed anti-biofilm systems have failed due to insufficient antibiotic delivery when applied to bacterial plaque, particularly biofilm isolated from drug administration. In addition, the lack of transfer from the outer layer may lead to lower antibacterial drug infiltration. The standard treatment strategies for periodontal disease include periodontal curettage, root scaling, and planning combined with the application of antibiotics, like tetracycline hydrochloride, doxycycline, and minocycline, which can help control bacterial infection. Nevertheless, not all antibiotic drugs can reach the base of deeper pockets in the gum tissue due to the low permeability resulting from embedding the microorganisms and their metabolic products into a highly-organized intercellular matrix and a complex microbial community.[48–50] There are several strategies to inhibit the oral biofilm, such as blocking the bacterial growth with antibiotics, mechanically disrupting the established dental plaque, modifying the biofilm infiltrate portrait, and delivering effective antimicrobials. However, some reports suggested that standard methods cannot inhibit biofilm development entirely because bacteria can escape from regular cleaning and restore plaque growth.

Bacterial biofilms harbor high stiffness, forming a rigid wall that promotes pathogenicity by blocking antimicrobial agents and host defense. Moreover, biofilm microorganisms have been reported to be dramatically resistant to antibiotic treatment compared to the planktonic state. The residual bacterial biofilm provides nutrients for bacterial growth, allowing bacterial biofilm reproduction. Thus, eliminating bacterial biofilms is crucial in controlling and eradicating periodontal diseases. It is difficult for professional dental instruments or routine oral cleaning to eradicate bacterial biofilm.

The plaque biofilm contains different complexes of periodontal microorganisms and produces an extracellular polymeric matrix that prevents antibacterial drug delivery. Thus, investigations to promote the efficiency of drug penetration are vital.[51,52] Using nanoparticles in drug delivery offers several advantages over conventional treatments like scaling, root planning, antibiotics, and surgical intervention that may not be sufficient to eradicate the infection in severe cases. We chose the most common periodontal-associated planktonic bacteria, *S. sanguinis, F. nucleatum*, and *P. gingivalis*, to explore breaking the barrier of microorganisms plaque with nanoparticle drug delivery. Additionally, we used minocycline, Fe_3O_4, and Fe_3O_4@PDA as positive and negative controls for our experiments. Our results showed that these nanoparticles exhibited a robust antibacterial effect against *S. sanguinis, F. nucleatum*, and *P. gingivalis*. Interestingly, FPM treatment showed an inhibition effect similar to minocycline, suggesting that our proposed nano-drug carriers can successfully improve antibiotics' efficiency and reduce minocycline use to some extent.

Noticeably, it is universally acknowledged that the tricky step in treating periodontal disease is penetrating the biofilm by uncanny power. Hence, a magnetic field is applied to fight the menace of biofilms.[53,54] Our results showed that using FPM + MF significantly delivered antibacterial drugs to the target. After treatment, more dead bacteria (red signal) were detected in the biofilms of the FPM + MF group. Our in vitro results indicated that FPM + MF treatment worked to kill the three periodontal-associated bacterial biofilms. However, the biochemical composition, penetrating properties, and biofilm thickness in the patient may be distinct. Therefore, we explored the effect of magnetic nano-drug carriers on a rat periodontitis model. HE staining images showed that rat gingival tissue had no inflammatory cell infiltration in the FMP + MF group, implying magnetic nano-drug delivery works successfully on rats under the magnetic targeting force. Pro-inflammatory cytokines, particularly IL-1β, IL-6, and TNF-α, are essential components of the host immune response.[55,56] The anti-inflammation effects were further confirmed by qRT-PCR and Western blot, where the periodontitis model group displayed the highest level of pro-inflammation marker at the mRNA and protein levels, which were dramatically reduced by FPM + MF treatment. This suggests that FPM NPs can be driven into the deep and complex structure of the periodontal pocket under the motivation of the magnetic field and can penetrate deeply into the bacterial biofilm to eradicate it. The results of animal experiments in vivo suggest that the FPM + MF treatment could be an effective method for treating periodontitis.

There were several limitations in this study and its experimental approach. First, we only used a rat periodontitis model in this study; the human volunteer biofilm models of *S. sanguinis, P. gingivalis*, and *F. nucleatum* were insufficient to mimic the periodontitis conditions. Second, few bacterial species were tested in the present study, and we did not investigate the effects of FPM + MF on various combinations and concentrations of *S. sanguinis, P. gingivalis*, and *F. nucleatum*. Therefore, further studies are required to develop a natural biofilm as a periodontitis model. Last but not least, the study did not intensely investigate the potential mechanisms underlying the FPM + MF antibacterial effects. Despite the promising potential of nanoparticle drug delivery systems for periodontitis treatment, there are still challenges to overcome. Indeed, further research is required to optimize the size, shape, and surface of the nanoparticles to ensure effective targeting and drug release. In addition, addressing potential toxicity concerns and regulatory issues in clinical practice warrants further investigation.

Conclusion

In conclusion, Fe_3O_4@PDA@Mino magnetic nanocomposites possessing antibacterial and anti-inflammatory functions were designed and developed by self-polymerizing dopamine in situ at the surface of Fe_3O_4 NPs as a coating to load antibiotic minocycline. Experimental characterization demonstrated their desirable morphological attributes, core-shell structure, good dispersion, long-term stability, and excellent magnetic targeting ability. This core-shell structural design significantly enhances the loading efficiency of minocycline, which was confirmed by antibacterial experiments in vitro. Besides the antibacterial properties, FPM NPs held an admirable penetration ability against periodontal biofilms through magnetic-forced movement, enhancing their efficacy for biofilm removal. Pro-inflammatory markers measurement in a rat periodontitis model showed that FPM + MF treatment reduced IL-1β, IL-6, and TNF-α at the mRNA and protein levels, suggesting that the FPM + MF treatment can effectively relieve periodontal inflammation. Subgingival injection of FPM NPs combined with a magnetic field could efficiently deliver the magnetic nanomedicine into deep periodontal pockets and reduce inflammation in the periodontal by attacking and carrying the antibiotics into the biofilm and killing the bacteria.

Moreover, in vitro and in vivo studies have demonstrated the high biocompatibility and low systemic toxicity of FPM NPs. In conclusion, Fe_3O_4@PDA@Mino magnetic nanocomposites-based drug delivery systems have the potential to revolutionize periodontitis treatment by offering targeted, controlled, and efficient delivery of therapeutic agents. The treatment strategy of FPM NPs combined with a magnetic field is an effective method for treating clinical periodontitis.

Abbreviation

MNPs, Fe3O4 magnetic nanoparticles; FPM, Fe_3O_4@PDA@Mino; EPS, Extracellular polymeric substances; DMEM, Dulbecco's modified Eagle's Medium; Fe3O4@PDA NPs, Fe3O4 polydopamine nanoparticles; BHI, Brain Heart Infusion Broth; TEM, Transmission Electron Microscopy; SEM, Scanning Electron Microscope; DLS, Dynamic Light Scattering; CLSM, Confocal laser scanning microscopy.

Acknowledgments

All animal work was performed using protocols approved by the Institutional Animal Care and Use Committee of the Medical College of Nanchang University. This study was supported by funding from National Natural Science Foundation of China (No. 82060198), Natural Science Foundation of Jiangxi province (No. 20192BAB205055, 20224BAB216078) and Scientific research project of Jiangxi Provincial Department of Education (No. G55210197). We sincerely thank Yunyun Deng for for technical assistance in performing PCR and Western blot assays. We thank Jing Pei, and Yunxiang Jia for assistance in histopathological examination.

Author Contributions

All authors made a significant contribution to the work reported, whether that is in the conception, study design, execution, acquisition of data, analysis and interpretation, or in all these areas; took part in drafting, revising or critically reviewing the article; gave final approval of the version to be published; have agreed on the journal to which the article has been submitted; and agree to be accountable for all aspects of the work.

Funding

The present work was supported by the National Natural Science Foundation of China (82060198), Natural Science Foundation of Jiangxi Province of China (20192BAB205055, 20224BAB216078) and Scientific research project of Jiangxi Provincial Department of Education (No. G55210197).

Disclosure

The authors report no commercial, proprietary, or financial interest in the products or companies described in this article. The authors declare no competing financial interests.

References

1. Johnston W, Rosier BT, Artacho A, et al. Mechanical biofilm disruption causes microbial and immunological shifts in periodontitis patients. *Sci Rep*. 2021;11(1):9796. doi:10.1038/s41598-021-89002-z
2. Hoare A, Soto C, Rojas-Celis V, et al. Chronic inflammation as a link between periodontitis and carcinogenesis. *Mediators Inflamm*. 2019;2019:1029857. doi:10.1155/2019/1029857
3. Kinane DF, Stathopoulou PG, Papapanou PN. Periodontal diseases. *Nat Rev Dis Primers*. 2017;3(1):17038. doi:10.1038/nrdp.2017.38
4. Fagundes NCF, Almeida A, Vilhena KFB, Magno MB, Maia LC, Lima RR. Periodontitis as a risk factor for stroke: a systematic review and meta-analysis. *Vasc Health Risk Manag*. 2019;15:519–532. doi:10.2147/VHRM.S204097
5. Shiga Y, Hosomi N, Nezu T, et al. Association between periodontal disease due to Campylobacter rectus and cerebral microbleeds in acute stroke patients. *PLoS One*. 2020;15(10):e0239773. doi:10.1371/journal.pone.0239773
6. Khosravi Samani M, Jalali F, Seyyed Ahadi SM, Hoseini SR, Dabbagh Sattari F. The relationship between acute myocardial infarction and periodontitis. *Caspian J Intern Med*. 2013;4(2):667–671.
7. Perk J, De Backer G, Gohlke H, et al. European guidelines on cardiovascular disease prevention in clinical practice (version 2012): the Fifth Joint Task Force of the European Society of Cardiology and Other Societies on Cardiovascular Disease Prevention in Clinical Practice (constituted by representatives of nine societies and by invited experts) Developed with the special contribution of the European Association for Cardiovascular Prevention & Rehabilitation (EACPR). *Eur Heart J*. 2012;33(13):1635–1701. doi:10.1093/eurheartj/ehs254
8. Surma S, Romańczyk M, Witalińska-łabuzek J, Czerniuk MR, Łabuzek K, Filipiak KJ. Periodontitis, blood pressure, and the risk and control of arterial hypertension: epidemiological, clinical, and pathophysiological aspects-review of the literature and clinical trials. *Curr Hypertens Rep*. 2021;23(5):27. doi:10.1007/s11906-021-01140-x
9. Leong X-F, Ng C-Y, Badiah B, Das S. Association between hypertension and periodontitis: possible mechanisms. *Scient World J*. 2014;2014:768237. doi:10.1155/2014/768237
10. Michaud DS, Izard J. Microbiota, oral microbiome, and pancreatic cancer. *Cancer J*. 2014;20(3):203–206. doi:10.1097/PPO.0000000000000046
11. Nwizu N, Wactawski-Wende J, Genco RJ. Periodontal disease and cancer: epidemiologic studies and possible mechanisms. *Periodontol 2000*. 2020;83(1):213–233. doi:10.1111/prd.12329
12. Marsh PD, Devine DA. How is the development of dental biofilms influenced by the host? *J Clin Periodontol*. 2011;38(s11):28–35. doi:10.1111/j.1600-051X.2010.01673.x
13. Haney EF, Trimble MJ, Cheng JT, Vallé Q, Hancock REW. Critical assessment of methods to quantify biofilm growth and evaluate antibiofilm activity of host defence peptides. *Biomolecules*. 2018;8(2):29. doi:10.3390/biom8020029
14. Roy R, Tiwari M, Donelli G, Tiwari V. Strategies for combating bacterial biofilms: a focus on anti-biofilm agents and their mechanisms of action. *Virulence*. 2018;9(1):522–554. doi:10.1080/21505594.2017.1313372
15. Lasserre JF, Brecx MC, Toma S. Oral microbes, biofilms and their role in periodontal and peri-implant diseases. *Materials*. 2018;11(10):1802. doi:10.3390/ma11101802
16. Allaker RP. *Nanobiomaterials in Clinical Dentistry*. Netherlands: Elsevier; 2013.

17. Yazdanian M, Rostamzadeh P, Rahbar M, et al. The potential application of green-synthesized metal nanoparticles in dentistry: a comprehensive review. *Bioinorg Chem Appl*. 2022;3:2311910. doi:10.1155/2022/2311910
18. Hakim LK, Yazdanian M, Alam M, et al. Biocompatible and biomaterials application in drug delivery system in oral cavity. *Evid Based Complementary Altern Med*. 2021;13:9011226. doi:10.1155/2021/9011226
19. Tahmasebi E, Keshvad A, Alam M, et al. Current infections of the orofacial region: treatment, diagnosis, and epidemiology. *Life*. 2023;13(2):269. doi:10.3390/life13020269
20. Wang P, Wang L, Zhan Y, et al. Versatile hybrid nanoplatforms for treating periodontitis with chemical/photothermal therapy and reactive oxygen species scavenging. *Chem Eng J*. 2023;463:142293. doi:10.1016/j.cej.2023.142293
21. Yazdanian M, Rostamzadeh P, Alam M, et al. Evaluation of antimicrobial and cytotoxic effects of Echinacea and Arctium extracts and Zataria essential oil. *AMB Express*. 2022;12(1):75. doi:10.1186/s13568-022-01417-7
22. Moghaddam A, Ranjbar R, Yazdanian M, et al. The current antimicrobial and antibiofilm activities of synthetic/herbal/biomaterials in dental application. *Biomed Res Int*. 2022;2:8856025. doi:10.1155/2022/8856025
23. Decho AW, Gutierrez T. Microbial Extracellular Polymeric Substances (EPSs) in ocean systems. *Front Microbiol*. 2017;26(8):922. doi:10.3389/fmicb.2017.00922
24. Di Martino P. Extracellular polymeric substances, a key element in understanding biofilm phenotype. *AIMS Microbiol*. 2018;4(2):274–288. doi:10.3934/microbiol.2018.2.274
25. Mishra R, Panda AK, De Mandal S, Shakeel M, Bisht SS, Khan J. Natural anti-biofilm agents: strategies to control biofilm-forming pathogens. *Front Microbiol*. 2020;29(11):566325. doi:10.3389/fmicb.2020.566325
26. Furner-Pardoe J, Anonye BO, Cain R, et al. Anti-biofilm efficacy of a medieval treatment for bacterial infection requires the combination of multiple ingredients. *Sci Rep*. 2020;10(1):12687. doi:10.1038/s41598-020-69273-8
27. Hwang G, Paula AJ, Hunter EE, et al. Catalytic antimicrobial robots for biofilm eradication. *Sci Robot*. 2019;4(29):eaaw2388. doi:10.1126/scirobotics.aaw2388
28. Shkodenko L, Kassirov I, Koshel E. Metal oxide nanoparticles against bacterial biofilms: perspectives and limitations. *Microorganisms*. 2020;8(10):1545. doi:10.3390/microorganisms8101545
29. Subbiahdoss G, Sharifi S, Grijpma DW, et al. Magnetic targeting of surface-modified superparamagnetic iron oxide nanoparticles yields antibacterial efficacy against biofilms of gentamicin-resistant staphylococci. *Acta Biomaterialia*. 2012;8(6):2047–2055. doi:10.1016/j.actbio.2012.03.002
30. Li J, Nickel R, Wu J, Lin F, van Lierop J, Liu S. A new tool to attack biofilms: driving magnetic iron-oxide nanoparticles to disrupt the matrix. *Nanoscale*. 2019;11(14):6905–6915. doi:10.1039/c8nr09802f
31. Taylor EN, Kummer KM, Durmus NG, Leuba K, Tarquinio KM, Webster TJ. Superparamagnetic iron oxide nanoparticles (SPION) for the treatment of antibiotic-resistant biofilms. *Small*. 2012;8(19):3016–3027. doi:10.1002/smll.201200575
32. Sun X, Sun J, Sun Y, et al. Oxygen self-sufficient nanoplatform for enhanced and selective antibacterial photodynamic therapy against anaerobe-induced periodontal disease. *Adv Funct Mater*. 2021;31(20):2101040. doi:10.1002/adfm.202101040
33. Quan K, Jiang G, Liu J, et al. Influence of interaction between surface-modified magnetic nanoparticles with infectious biofilm components in artificial channel digging and biofilm eradication by antibiotics in vitro and in vivo. *Nanoscale*. 2021;13(8):4644–4653. doi:10.1039/d0nr08537e
34. Quan K, Zhang Z, Ren Y, Busscher HJ, van der Mei HC, Peterson BW. Homogeneous distribution of magnetic, antimicrobial-carrying nanoparticles through an infectious biofilm enhances biofilm-killing efficacy. *ACS Biomater Sci Eng*. 2020;6(1):205–212. doi:10.1021/acsbiomaterials.9b01425
35. Quan K, Zhang Z, Chen H, et al. Artificial channels in an infectious biofilm created by magnetic nanoparticles enhanced bacterial killing by antibiotics. *Small*. 2019;15(39):1902313. doi:10.1002/smll.201902313
36. Uskoković V, Pejčić A, Koliqi R, Anđelković Z. Polymeric nanotechnologies for the treatment of periodontitis: a chronological review. *Int J Pharm*. 2022;625:122065. doi:10.1016/j.ijpharm.2022.122065
37. Jin A, Wang Y, Lin K, et al. Nanoparticles modified by polydopamine: working as "drug" carriers. *Bioactive Mater*. 2020;5(3):522–541. doi:10.1016/j.bioactmat.2020.04.003
38. Steckiewicz KP, Cieciórski P, Barcińska E, et al. Silver nanoparticles as chlorhexidine and metronidazole drug delivery platforms: their potential use in treating periodontitis. *Int J Nanomedicine*. 2022;17:495–517. doi:10.2147/IJN.S339046
39. Shi E, Bai L, Mao L, et al. Self-assembled nanoparticles containing photosensitizer and polycationic brush for synergistic photothermal and photodynamic therapy against periodontitis. *J Nanobiotechnology*. 2021;19(1):413. doi:10.1186/s12951-021-01114-w
40. Baghban A, Jabbari M, Rahimpour E. Fe3O4@polydopamine core-shell nanocomposite as a sorbent for efficient removal of rhodamine b from aqueous solutions: kinetic and equilibrium studies. *Iran J Chem Chem Eng*. 2018;37(1):17–28.
41. Mercado N, Bhatt P, Sutariya V, Florez FLE, Pathak YV. *Surface Modification of Nanoparticles for Targeted Drug Delivery*. Switzerland: Springer International Publishing; 2019.
42. Liu M, Yu W, Zhang F, et al. Fe(3)O(4)@polydopamine-labeled MSCs targeting the spinal cord to treat neuropathic pain under the guidance of a magnetic field. *Int J Nanomedicine*. 2021;11(16):3275–3292. doi:10.2147/IJN.S296398
43. Mercado N, Bhatt P, Sutariya V, Florez FLE, Pathak YV. *Application of Nanoparticles in Treating Periodontitis: Preclinical and Clinical Overview*. Springer International Publishing: Switzerland; 2019.
44. Kang W, Jia Z, Tang D, et al. Fusobacterium nucleatum facilitates apoptosis, ROS generation, and inflammatory cytokine production by activating AKT/MAPK and NF-κB signaling pathways in human gingival fibroblasts. *Oxid Med Cell Longev*. 2019;2019:1681972. doi:10.1155/2019/1681972
45. Hajishengallis G, Chavakis T. Local and systemic mechanisms linking periodontal disease and inflammatory comorbidities. *Nat Rev Immunol*. 2021;21(7):426–440. doi:10.1038/s41577-020-00488-6
46. Vestby LK, Grønseth T, Simm R, Nesse LL. Bacterial biofilm and its role in the pathogenesis of disease. *Antibiotics*. 2020;9(2):59. doi:10.3390/antibiotics9020059
47. Srinivasan R, Santhakumari S, Poonguzhali P, Geetha M, Dyavaiah M, Xiangmin L. Bacterial biofilm inhibition: a focused review on recent therapeutic strategies for combating the biofilm mediated infections. *Front Microbiol*. 2021;12. doi:10.3389/fmicb.2021.676458.
48. Rath S, Bal SCB, Dubey D. Oral biofilm: development mechanism, multidrug resistance, and their effective management with novel techniques. *Rambam Maimonides Med J*. 2021;12(1):e0004. doi:10.5041/RMMJ.10428

49. Kanwar I, Sah AK, Suresh PK. Biofilm-mediated antibiotic-resistant oral bacterial infections: mechanism and combat strategies. *Curr Pharm Des*. 2017;23(14):2084–2095. doi:10.2174/1381612822666161124154549
50. Sharma D, Misba L, Khan AU. Antibiotics versus biofilm: an emerging battleground in microbial communities. *Antimicrob Resist Infect Control*. 2019;8(1):76. doi:10.1186/s13756-019-0533-3
51. Hughes G, Webber MA. Novel approaches to the treatment of bacterial biofilm infections. *Br J Pharmacol*. 2017;174(14):2237–2246. doi:10.1111/bph.13706
52. Bi Y, Xia G, Shi C, et al. Therapeutic strategies against bacterial biofilms. *Fundamental Res*. 2021;1(2):193–212. doi:10.1016/J.FMRE.2021.02.003
53. Gao L, Giglio KM, Nelson JL, Sondermann H, Travis AJ. Ferromagnetic nanoparticles with peroxidase-like activity enhance the cleavage of biological macromolecules for biofilm elimination. *Nanoscale*. 2014;6(5):2588–2593. doi:10.1039/c3nr05422e
54. Sun Y, Sun X, Li X, et al. A versatile nanocomposite based on nanoceria for antibacterial enhancement and protection from aPDT-aggravated inflammation via modulation of macrophage polarization. *Biomaterials*. 2021;268:120614. doi:10.1016/j.biomaterials.2020.120614
55. Xi L, Wang C, Chen P, et al. Expressions of IL-6, TNF-α and NF-κB in the skin of Chinese brown frog (Rana dybowskii). *Eur J Histochem*. 2017;61(4):2834. doi:10.4081/ejh.2017.2834
56. Arango Duque G, Descoteaux A. Macrophage Cytokines: involvement in Immunity and Infectious Diseases. *Front Immunol*. 2014;7(5):491. doi:10.3389/fimmu.2014.00491